NANO · MICRO small
www.small-journal.com

Check for updates

Analytical Photoresponses of Schottky-Contact MoS_2 Phototransistors

Jianyong Wei, Yumeng Liu, Yizhuo Wang, Kai Li, Zhentao Lian, Maosong Xie, Xinhan Yang, Seyed Saleh Mousavi Khaleghi, Fuxing Dai, Weida Hu, Xuejiao Gao, Rui Yang,* and Yaping Dan**

High-gain photodetectors based on 2D semiconductors have been extensively investigated in the past decades. However, the underlying mechanism remains in dispute without a proper analytical theory. On one side, the classical photogain theory is not applicable, as it was derived on two misplaced assumptions. On the other side, unexpected potential barriers usually present in 2D semi-conductors but their effect on the ultrahigh gain has been largely ignored. In this work, we first established a universal *I-V* equation for Schottky-contact MoS_2 phototransistors, modeled with two anti-symmetric Schottky diodes and a channel resistor in series. It has been proved to be valid under varying conditions of gate voltage, temperature, light illumination and bias voltage. Moreover, we established analytical equations for photocurrent and gain, which clearly shows that ultrahigh gain is created by light-induced modulation of potential barrier in exponential form. Finally, the theory was validated on 40 samples by verifying the *I–V* characteristics and minority carrier lifetime. Our results not only shed light on the working mechanism of 2D phototransistors, but also present important advance for device modeling and design in 2D integrated circuits.

1. Introduction

Low-dimensional photodetectors often have extraordinarily high photogain (up to 10^{10}).[1–5] It was believed in the classical photogain theory that the gain comes from the recycling of photogenerated charge carriers, i.e., photogenerated electrons or holes, driven by electric fields, circulate in the circuit multiple times before recombination.[6–10] In fact, photogenerated electrons and holes in a doped semiconducting photoconductor cannot be spatially separated due to the ambipolar transport.[11] In recent years, we found that the classical theory was derived on two misplaced assumptions.[12] The first assumption is that the photogenerated excess carriers are uniform in spatial distribution on condition of uniform doping and illumination. This assumption is actually invalid due to the confinement of metal-semiconductor boundary. The second assumption is that the excess electrons and holes have an equal contribution to the photocurrent, which intuitively should be true because the absorption of photons will create an equal number of electrons and holes. However, devices in practice often have surfaces or interfaces where depletion regions and/or trap states appear. The depletion regions and/or trap states will localize excess minority carriers, leaving the majority counterparts to dominantly contribute to the photocurrent.

After correcting these two assumptions, we further derived the explicit gain equations for single crystalline nanowires based on photo Hall measurements.[13,14] The derived photo gain equation is a function of incident light intensity with several important physical parameters including nanowire size, doping concentration, and depletion width of surface. According to the fitting results with experimental data, significant physical parameters, such as minority carrier recombination lifetime, are extracted and consistent with previously reported results.[15,16] Similar to the classical theory, the derived photo gain is still proportional to the ratio of minority recombination lifetime to transit time. However, the limited value of this ratio (usually less than 10) is proven not the origin of the high photo gain (10^6–10^8), which actually originates from the modulation of the

J. Wei, Y. Liu, Y. Wang, K. Li, Z. Lian, M. Xie, S. S. M. Khaleghi, R. Yang, Y. Dan
State Key Laboratory of Advanced Optical Communication Systems and Networks
University of Michigan – Shanghai Jiao Tong University Joint Institute
Shanghai Jiao Tong University
Shanghai 200240, China
E-mail: rui.yang@sjtu.edu.cn; Yaping.dan@sjtu.edu.cn

X. Yang, X. Gao
Hebei Key Laboratory of Physics and Energy Technology
Department of Mathematics and Physics
North China Electric Power University
Baoding, Hebei 071003, China
E-mail: gaoxuejiao@ncepu.edu.cn

F. Dai, W. Hu
State Key Laboratory of Infrared Physics
Shanghai Institute of Technical Physics
Chinese Academy of Sciences
Shanghai 200083, China

R. Yang
State Key Laboratory of Radio Frequency Heterogeneous Integration
Shanghai Jiao Tong University
Shanghai 200240, China

The ORCID identification number(s) for the author(s) of this article can be found under https://doi.org/10.1002/smll.202408508

DOI: 10.1002/smll.202408508

 © 2024 Wiley-VCH GmbH

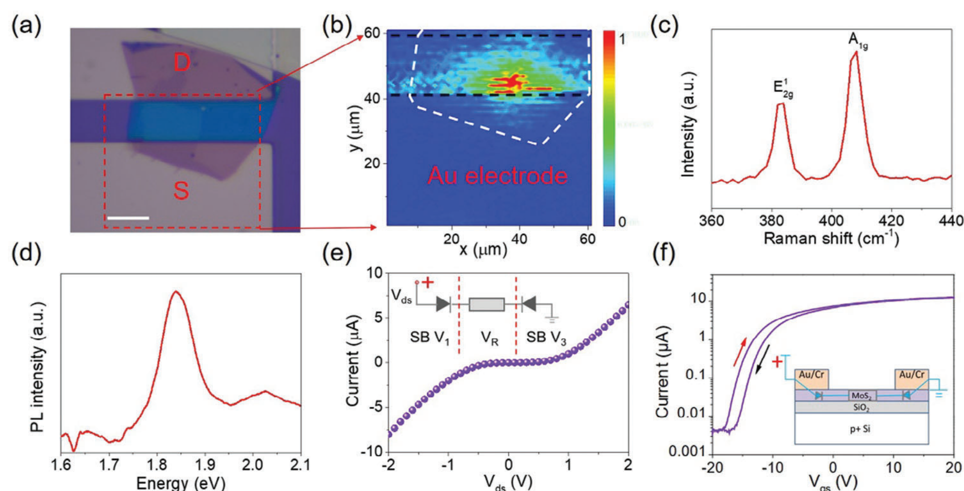

Figure 1. a) Optical microscopic image of a MoS_2 device. The scale bar is 20 μm. b) Scanning photocurrent microscopy of the MoS_2 device. The laser beam power is ≈500 μW and beam size is ≈2μm. c) Raman shifts and d) photoluminescence spectrum of the multilayer MoS_2. e) *I–V* characteristics of the MoS_2 device. Inset: device model of the Schottky contact MoS_2. f) Gate transfer characteristics of the MoS_2 transistor with V_{ds} = 2 V. The inset is the schematic diagram of the phototransistor.

conduction channel width by photovoltage across the surface depletion region.

2D semiconductors, particularly 2D MoS_2, have emerged as a promising candidate for integrated circuits to supplement Si.[17,18] The development of explicit device theories for 2D semiconducting devices is crucial for integrated circuits (IC) based on 2D materials as the modern IC industry heavily relies on circuit design and modeling due to the astronomical scale of circuits. Although photodetectors based on 2D semiconductors have been extensively investigated,[3,4,19–24] there is no analytical theory that governs the photoresponses of these devices, and the effects from the Schottky contact in 2D phototransistors have been largely ignored in the past decades. Nevertheless, metal in contact with 2D semiconductors often forms a Schottky junction unless a proper metal is chosen to align the work function of metals and 2D semiconductors. Meanwhile the choice of metals is quite limited due to the compatibility issue in the complicated IC fabrication process, other traditional approaches to form Ohmic contacts such as high doping to facilitate quantum tunneling and thermal annealing to form metal-semiconductor alloys are not applicable for atomically thin 2D semiconductors. Schottky contact 2D semiconducting devices may be ubiquitous in ICs based on 2D materials. Therefore, it is important to decipher the underlying mechanism and establish an explicit device theory for Schottky contact MoS_2 transistors and photodetectors.

Inspired by our previous work on high-gain photoconductors,[13,14] we derived explicit analytical equations for *I–V* characteristics, photocurrent and photogain, and thus developed an ultrahigh gain theory for Schottky-contact MoS_2 phototransistors. According to our theory, parameters like voltage drop can be extracted from *I–V* characteristics and working mechanism of 2D transistors can be easily judged to be Schottky-diode-dominant or channel-related-resistor-dominant. In addition, we found in this work that high-gain photoresponses in Schottky contact MoS_2 photodetectors are created by the light-induced modulation of Schottky barrier ($\Delta\Phi$) in exponential form. To validate the analytical photoresponse model, we extracted the minority recombination lifetimes by fitting *I–V* curves with analytical photoresponse model. The values are largely comparable with value from the transient photoluminescence measurements. To check the universality of our theory, we fabricated ≈40 MoS_2 devices with either Schottky–Schottky junctions or Schottky-Ohmic junctions. The measured characteristics of these devices are all fitted well with our theory. This work represents an important advance for device modeling and design in integrated circuits based on 2D semiconductors.

2. Results and Discussion

The optical image of the back-gate MoS_2 field effect transistor (FET) is shown in **Figure 1a**, from which we can see that the multilayer MoS_2 is on top of and in good contact with both electrodes. The device was fabricated following the procedure as described below. Two Au/Cr electrodes were first formed on p^+-Si/SiO_2 wafer (300 nm thick SiO_2) by photolithography and thermal evaporation. As the next step, a multilayer MoS_2 flake was mechanically exfoliated from a bulk MoS_2 and then dry-transferred onto the target surface in contact with the electrodes. Finally, the device was annealed in vacuum at 300 °C for 30 min. The channel is ≈20 μm long and ≈64 μm wide. Figure 1b shows the scanning photocurrent mapping of the device, which we will discuss later.

The material quality of the exfoliated MoS_2 flakes was examined with Raman and photoluminescence spectroscopy. As shown in Figure 1c, two Raman peaks at 383.9 and 408.3 cm^{-1} were observed, which are the E^1_{2g} and A_{1g} vibration mode of MoS_2, respectively. It is known that the separation between E^1_{2g} and A_{1g} mode evolves with the number of MoS_2 layers. A peak separation of 24.4 cm^{-1} indicates that the flake is a few-layer MoS_2.[24] Photoluminescence (PL) characterizations were carried out under the

 © 2024 Wiley-VCH GmbH

16136829, 2025, 6, Downloaded from https://onlinelibrary.wiley.com/doi/10.1002/smll.202408508 by Yaping Dan - Shanghai Jiaotong University , Wiley Online Library on [14/02/2025]. See the Terms and Conditions (https://onlinelibrary.wiley.com/terms-and-conditions) on Wiley Online Library for rules of use; OA articles are governed by the applicable Creative Commons License

excitation of a 532 nm laser. The single strong PL peak at 1.84 eV was attained as shown in Figure 1d, indicating a good crystalline quality of the MoS_2 flake.

Schottky contacts often form between 2D materials and metal electrodes due to the Fermi level pinning at the interface and the mismatch in Fermi energy levels of the 2D material and metal. Recent researches found the strain-induced bandgap change of 2D materials is also an important reason for the formation of Schottky contacts.[25,26] It is well known that Schottky junctions play a dominant role in the electronic properties of semiconductor devices.[24–32] As a result, it is not surprising to see that the current–voltage characteristics of our device are nonlinear (Figure 1e). To double check the observation, we performed the scanning photocurrent microscopy (SPCM) on the device. In this measurement, a focused laser beam (λ = 532 nm) was used to scan over the MoS_2 device. Photocurrents and laser positions were then recorded simultaneously, forming a raster photocurrent map. The photocurrent map in Figure 1b (placed right next to the device image in Figure 1a for comparison) shows that the photocurrent of the MoS_2 device at a bias of 2 V is mainly located near the bottom Au electrode and extends well into the channel. This is because the Schottky junction near the bottom electrode is reverse biased and the top Schottky junction is at forward bias. At a bias of 2 V, the resistance of the forward Schottky junction is negligible. The reverse biased Schottky junction and channel are the main components in device resistance (see more discussions later) and therefore are the main sources of photocurrent in the map.

Figure 1f shows the gate-transfer characteristics of the MoS_2 device at a source-drain bias of 2V. At this bias, the MoS_2 channel dominates over the device resistance. As the gate voltage sweeps from 20 to −20 V, the source-drain current drops by 3 orders of magnitude, indicating that the MoS_2 channel is n-type. The hysteresis in gate transfer characteristics is attributed to the defects that trap or emit charges.

The *I–V* curve of a Schottky junction is governed by Equation (1):

$$I_0 = I_{s0}\, exp\left(-\frac{\phi}{kT}\right)\left[e^{\frac{qV}{kT}} - 1\right] \tag{1}$$

where ϕ is the Schottky barrier height (SBH), *k* is the Boltzmann constant, T is the temperature, and *V* is the applied voltage. I_{s0} is the current constant given by $I_{s0} = A^* T^{3/2} S$ for 2D semiconductors with A^* Being the Richardson constant, *S* the cross-sectional width of MoS_2 channel.

Schottky junctions of 2D materials in contact with metal, although fabricated in the same process, often have different *I-V* characteristics due to the dielectric disorder of 2D materials,[33] which is reflected in the difference of ideality factor and barrier height. More importantly, the Schottky barrier height of the 2D semiconductor can be modulated by the bias applied to the barrier following Equation. (2).[34]

$$\phi\ (V) = \phi_0\ \pm qV\left(1 - \frac{1}{n}\right) \tag{2}$$

where ϕ_0 is the intrinsic barrier height at zero bias, *V* the applied bias, *n* the ideal factor, and ± for forward and reverse bias, respectively. When we plug Equation. (2) into Equation. (1), we can rewrite the forward current as Equation (3a) and the reverse current as Equation (3b) after the term $e^{\frac{qV}{kT}} - 1$ is simplified as $e^{\frac{qV}{kT}}$ for forward bias and -1 for reverse bias, respectively, when |V|>3kT/q.

$$I_F = I_s\, exp\left(\frac{qV_F}{nkT}\right) \tag{3a}$$

$$I_R = -I_s \exp\left[\frac{qV_R}{kT}\left(1 - \frac{1}{n}\right)\right] \tag{3b}$$

in which $I_s = I_{s0}\ exp(-\frac{\emptyset_0}{kT})$, V_F is the forward bias, and V_R is the reverse bias.

Our device consists of two back-to-back Schottky junctions (#1 and #2) and one channel resistor *R* (as shown in the inset of Figure 1f). A bias voltage *V* will create a current flowing through the forward junction (#1), channel resistor, and reverse junction (#2). The bias voltage *V* will distribute among these three components in series, i.e., $V = V_{F1} + V_{R2} + R \times I$, which can be written as Equation (4) after plugging V_F for Junction #1 and V_R for Junction #2 found from Equation (3) (Note $I = I_F = -\ I_R$):

$$V = n_1 \frac{kT}{q} ln\left(\frac{I}{I_{s1}}\right) + \frac{n_2}{n_2 - 1}\frac{kT}{q} ln\left(\frac{I}{I_{s2}}\right) + RI \tag{4}$$

in which the subscript 1 and 2 represents the corresponding parameter of Junction #1 and #2, respectively. More specifically, $I_{s1} = I_{s01}\ exp(-\frac{\emptyset_{01}}{kT})$ and $I_{s2} = I_{s02}\ exp(-\frac{\emptyset_{02}}{kT})$. To make it convenient for fitting with experimental data, Equation (4) is reformatted into Equation (5) in which we use the current *I* as the variable and the bias voltage *V* as the function.

$$V = \left(n_1 + \frac{n_2}{n_2 - 1}\right)\frac{kT}{q} ln\frac{I}{I_s^e} + RI \tag{5}$$

where $I_s^e = {I_{s1}}^{\alpha}\ {I_{s2}}^{\beta}$ with $\alpha = n_1\ /(n_1 + \frac{n_2}{n_2-1})$ and $\beta = \frac{n_2}{n_2-1}\ /(n_1 + \frac{n_2}{n_2-1})$. The derived Equation (5) governs *I–V* characteristics of back-to-back MoS_2 Schottky junctions, which is universal for other 2D semiconductor devices in Schottky contact.

We plot the bias voltage (V_{ds}) versus current (*V–I*) characteristics at different gate voltage. Excitingly, the *V–I* characteristics in **Figure 2a** can be nicely fitted with Equation (5), from which we extracted the leakage current I_S (calculated from the extracted I_s^e, see Table S1 and Section I, Supporting Information) for the two Schottky junctions and the channel resistance *R*. Figure 2b shows that the extracted leakage current I_{s1} and I_{s2} for Junction #1 and #2, respectively, which have a competing response to the gate voltage. Figure 2c plots the extracted channel resistances as a function of gate voltage. As expected, the channel resistance *R* extracted when V_{ds}>0V and V_{ds}<0 V are comparable, which validates our device model. The channel resistance R is less dependent on gate voltage because trap states compromise the gating effect on the channel. What's more, the extracted ideality factor n_1 and n_2 are both slightly larger than 1 (see Figure S1a and Section I, Supporting Information), which is reasonable because of the thermally-assisted tunneling in Schottky junctions.

 © 2024 Wiley-VCH GmbH

16136829, 2025, 6, Downloaded from https://onlinelibrary.wiley.com/doi/10.1002/smll.202408508 by Yaping Dan - Shanghai Jiaotong University , Wiley Online Library on [14/02/2025]. See the Terms and Conditions (https://onlinelibrary.wiley.com/terms-and-conditions) on Wiley Online Library for rules of use; OA articles are governed by the applicable Creative Commons License

16136829, 2025, 6, Downloaded from https://onlinelibrary.wiley.com/doi/10.1002/smll.202408508 by Yaping Dan - Shanghai Jiaotong University , Wiley Online Library on [14/02/2025]. See the Terms and Conditions (https://onlinelibrary.wiley.com/terms-and-conditions) on Wiley Online Library for rules of use; OA articles are governed by the applicable Creative Commons License

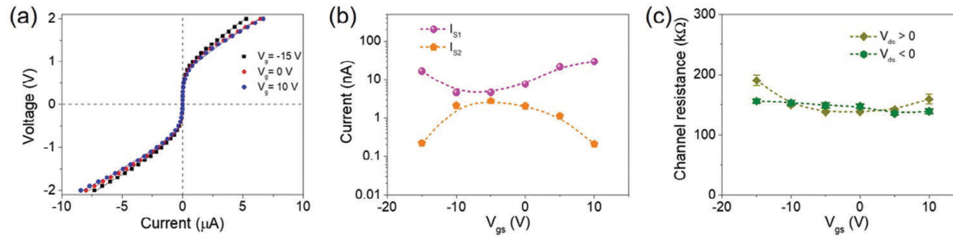

Figure 2. a) Gate-dependent *V–I* characteristics fitted with Equation (5). b) Extracted the leakage current I_{s1} (purple diamonds) and I_{s2} (Orange dots) for the two Schottky junctions. c) Extracted channel resistances for source-drain bias greater (brown diamonds) and less than zero (green dots).

Figure 3 shows the temperature dependent *V–I* characteristics for V_{ds}>0V and V_{ds}<0 V which can be also well fitted with Equation (5). According to the fittings, we extracted the leakage currents and channel resistances as a function of temperature, as shown in Figure 3b,c, respectively. The leakage currents for both junctions increase as the temperature rises, but with different correlations. It is worthy to point out that we cannot extract the intrinsic Schottky barrier height ϕ_0 from the leakage currents I_{s1} or I_{s2} because the Richardson constant in I_{s0} is temperature dependent (see Figure S2 and Section II, Supporting Information). This fact indicates that the metal-MoS_2 Schottky junction shall be modeled with the mixed thermionic emission and diffusion model developed by Crowell and Sze,[35] in which the Richardson constant is implicitly dependent on temperature. Moreover, the temperature dependent Richardson constant also explains why the channel resistances R calculated with V_{ds} >0 and V_{ds}<0 deviate from each other as the temperature reduces to 175 K or lower.

Based on the device theory above, we investigated the working mechanism and analytical photoresponses of the MoS_2 phototransistor. First, we recorded the *I–V* characteristics (a different device) under the illumination of light (λ = 525 nm) with different intensities (**Figure 4a**). All the five *I–V* curves with light intensity increasing from 0 to 24 mW cm^{-2} are well fitted with Equation (5). The derived voltage load on Junction #1 (V_1), Junction #2 (V_3) and channel resistance (V_R) as a function of source-drain bias are shown in Figure 4b. At bias voltage higher than 1.8 V, the channel resistance dominates the source-drain resistance. But as the bias is lower than 1.8 V, the reverse biased Schottky junction (here junction #2) play a leading role. Under light illumination, the photoresponse of reverse biased Schottky junction keeps predominant. This photoresponse is ascribed to the reduction $\Delta\phi$ of the intrinsic Schottky barrier height ϕ_{02}. Therefore, we have the total current under light illumination shown in Equation (6).

$$I_L = -I_{s0} exp\left(-\frac{\emptyset_{02} - \Delta\phi}{kT}\right)\ \exp\left[\frac{qV_R}{kT}\left(1 - \frac{1}{n}\right)\right] = I_{dark}\ exp\left(\frac{\Delta\phi}{kT}\right) \quad (6)$$

Previously, we found that the nanowire channel will be pinched off when the nanowire is narrower than two times of the surface depletion region width in the nanowire. In this case, a potential barrier exists between the source and drain. Light illumination will reduce the potential barrier, inducing a photocurrent. The light intensity and the potential barrier reduction is correlated following Equation (7).[14,36] Schottky contact MoS_2 phototransistor in this work is quite similar, with a potential barrier from the predominant reverse biased Schottky junction. At a fixed bias, light illumination will also reduce this potential barrier (see Figure 4c). The potential barrier reduction $\Delta\phi$ can be calculated from the current in darkness and under light illumination following Equation (6). Figure 4d shows $\Delta\phi$ as a function of light intensity at different bias which can be nicely fitted with Equation (7). The fitting results are consistent with what will be presented later in **Figure 5**.

$$P_{light} = P^S_{light}\ \left[exp\left(\frac{\Delta\emptyset}{mkT}\right) - 1\right] \quad (7)$$

where m is the ideality factor determining how effectively the potential barrier is reduced by light illumination. It depends on the device structure, light absorption, defects in the junction, and others. P^S_{light} is defined as the critical light intensity which is given by $P^S_{light} = \frac{\hbar\omega n_i}{2\alpha\tau_0}$, in which $\hbar\omega$ is the photon energy, n_i Is the

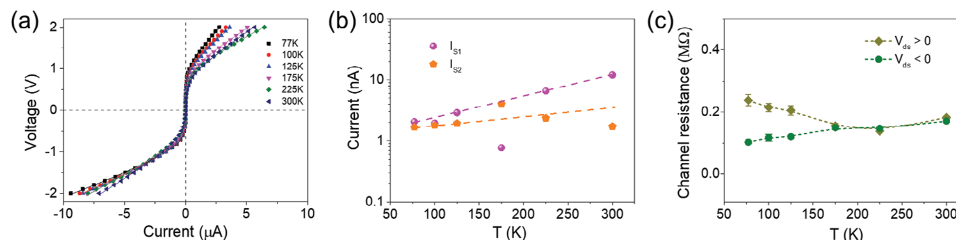

Figure 3. a) Temperature-dependent *V–I* characteristics fitted with Equation (5). b) Extracted the leakage current Is_1 (purple diamonds) and Is_2 (Orange dots) for the two Schottky junctions. c) Extracted channel resistances for source-drain bias that is greater (brown diamonds) and less than zero (green dots).

 © 2024 Wiley-VCH GmbH

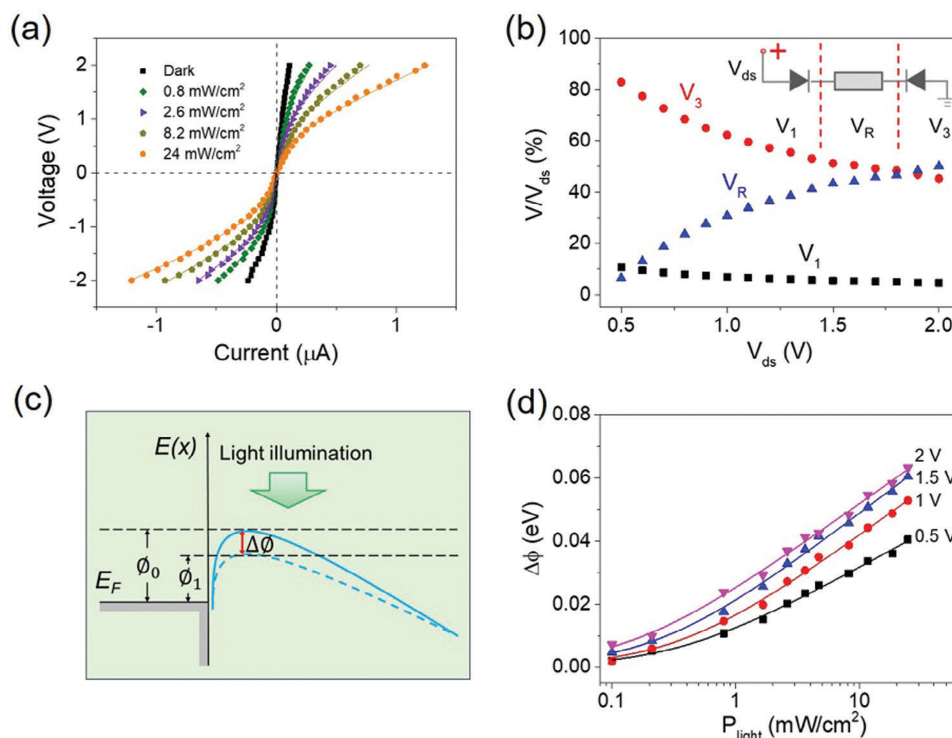

Figure 4. a) V–I characteristics under light illumination ($\lambda = 525$ nm) of different intensity. b) Voltage drops on the forward and reverse biased Schottky Junction, and the MoS_2 channel in darkness. c) Schematic diagram of the energy band structure of Schottky barrier under light illumination. d) Schottky barrier reduction as a function of light illumination for different bias.

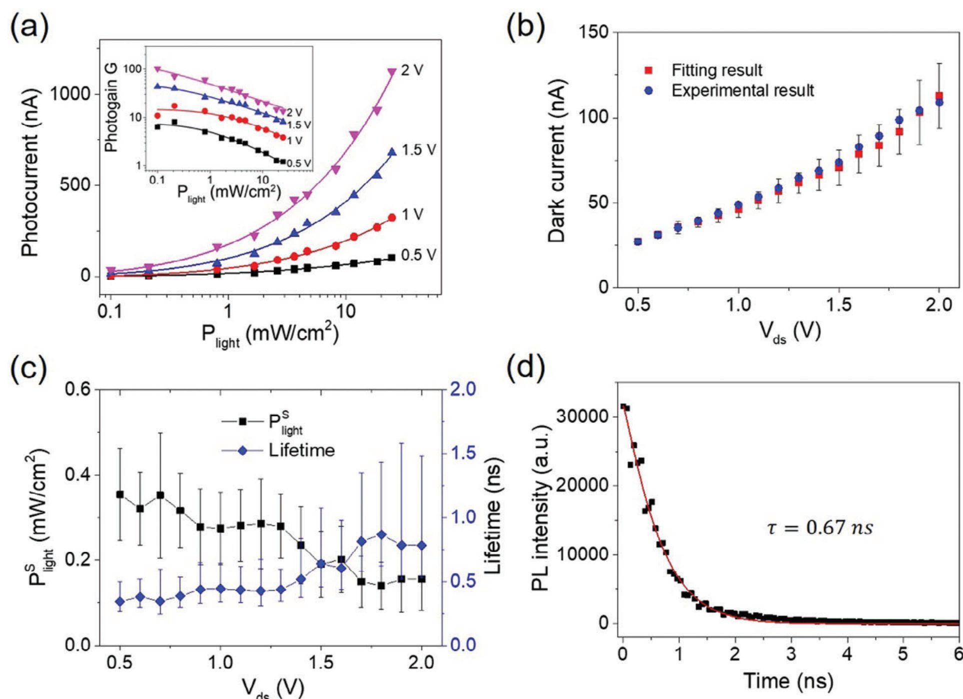

Figure 5. a) Photocurrent dependent on light intensity at different source-drain bias. Inset: photogain as a function of light intensity at different source-drain bias. b) Experimental and extracted dark current versus source-drain bias. c) The extracted critical light intensity P^S_{light} and minority carrier lifetime τ_0 versus source-drain bias. d) Transient photoluminescence of the MoS_2 flake.

© 2024 Wiley-VCH GmbH

16136829, 2025, 6, Downloaded from https://onlinelibrary.wiley.com/doi/10.1002/smll.202408508 by Yaping Dan - Shanghai Jiaotong University , Wiley Online Library on [14/02/2025]. See the Terms and Conditions (https://onlinelibrary.wiley.com/terms-and-conditions) on Wiley Online Library for rules of use; OA articles are governed by the applicable Creative Commons License

intrinsic electron concentration (per unit area) of MoS_2, α is the light absorption ratio by MoS_2 and τ_0 is the minority recombination lifetime in MoS_2.

From Equations (6) and (7), we find that the total current under light illumination is dependent on the illumination light intensity P_{light} following Equation (8).

$$I_L = I_{ph} + I_{dark} = I_{dark}\left(\frac{P_{light}}{P^S_{light}} + 1\right)^m \tag{8}$$

Furthermore, the photogain (G) shown in Equation (9) can be derived from Equation (8).

$$G = \frac{I_{ph}/q}{P_{light}WL/\hbar\omega} = G_{max}\left\{\frac{P^s_{light}}{mP_{light}}\left[\left(\frac{P_{light}}{P^s_{light}} + 1\right)^m - 1\right]\right\} \tag{9}$$

where $G_{max} = \frac{m\hbar\omega}{qP^s_{light}WL}$ is the maximum gain when the light intensity approaches to zero, and W and L represents the width and length of the MoS_2 channel.

Figure 5a along with the inset exhibits the experimental current of the MoS_2 device under light illumination and the corresponding photogain as a function of light intensity at different bias, which can be well fitted with Equations (8) and (9), respectively. In Equation (9), the photocurrent is normalized against the light intensity to derive the photogain. As a result, the photogain maximizes at weak light intensity. At weak light intensity, the signal-to-noise ratio is small for experimental data. A large uncertainty will be created if we use Equation (9) to fit the experimental data. For this reason, we use Equation (8) to perform our fittings (solid curves). At high bias (> 1.8 V in our case), although the channel resistance starts to dominate and the reverse biased Schottky junction become less important, the theory still fits well the experimental data. This indicates that the photoresponse of the MoS_2 channel also follows Equation (8). This is likely reasonable considering that there are defects in the atomically thin MoS_2 flake. These defects are charged, forming a potential barrier reducing the effective conduction channel width. Light illumination will reduce the potential barrier and create a photocurrent, following similar equations as shown in Equations (7) and (8).[37] A systematic investigation of the analytical photoresponses in the channel is subject to future work.

Here, let us focus on the fitting results of Equation (8). From the fittings, we extract the dark current I_{dark}, the ideality factor m and the critical light intensity P^S_{light}. The extracted dark currents are almost identical with the experimental value (Figure 5b), which validates the analytical photoresponse model. The extracted ideality factor m remains largely constant ≈0.35 to 0.48. To calculate the minority carrier recombination lifetime $\tau_0 = \frac{\hbar\omega n_i}{2\alpha P^S_{light}}$, we first find the photon energy of $\hbar\omega = 2.36\ eV$ for the incident light at a wavelength of 525 nm, and the absorption ratio of $\alpha = 41\%$ for a multilayered MoS_2 flake according to previous work.[38] The intrinsic electron concentration n_i of MoS_2 depends on the effective mass of electrons and holes. It is best estimated $n_i \approx 2.65 \times 10^5$ cm^{-2} (see section III, Supporting Information). Based on the extracted value and the expression of the critical light intensity P^S_{light} given above, we calculate the minority recombination lifetime of MoS_2 in a range of 0.3–1 ns as shown in Figure 5c. The minority recombination lifetime increases as the source-drain bias, likely because the photoresponse of the MoS_2 channel plays a more important role at higher voltage. Note that a metal in contact with a semiconductor will bring additional defects. Therefore, it is expected that the minority recombination lifetime is longer in the channel.

To further validate the analytical photoresponse, we experimentally measured the minority recombination lifetime. A pulsed laser illumination (λ = 405 nm) was employed to excite excess carriers in the MoS_2 flake. When the excitation pulse is switched to off state, the photoluminescence will exponentially decay following a stretched exponential decay function (Figure 5d).[39] Fitting the transient decay with this stretched exponential function, we find the minority carrier recombination lifetime as 0.67 ns, which is comparable with the lifetimes we extracted from the analytical photoresponses (Figure 5c), in particular when the MoS_2 channel resistance starts to dominate at high bias (> 1.8 V).

The gate voltage also has a significant impact on the photoresponse of the MoS_2 device. We recorded the total current under light illumination for different gate voltage as shown in **Figure 6a** (a different device). The current dependence on the light intensity can be nicely fitted with Equation (8) for all gate voltages. The extracted dark currents (black squares) are almost the same with the experimental ones (red dots) as shown in Figure 6b, suggesting that Equation (8) is valid for gated MoS_2 devices. From the extracted critical light intensity (black squares in Figure 6c), we found that the minority carrier recombination lifetime increases from ≈40 ps to ≈1 ns (blue diamonds) when the gate voltage sweeps from −10 to −20 V. The initial lifetimes are smaller by an order of magnitude than the ones presented in Figure 5 probably because this new MoS_2 flake is thinner or has a poorer quality than the previous one. At high negative gate voltage (< − 18 V), the minority recombination lifetime quickly increases likely due to the reduction of majority electrons in MoS_2 that suppresses the recombination rate of excess minority holes. Figure 6d plots the ideality factor m at different gate voltages. As the gate voltage sweeps from −10 to −20 V, m first remains nearly constant ≈0.3 and then increases to 0.5 after −18 V, exhibiting a pattern similar to the minority recombination lifetime in Figure 6c.

To verify the universality of this theory, we made ≈40 MoS_2 devices in the same process. A number of such devices with their electrical and optoelectrical characteristics are shown in Figure S3. The *I–V* curve and photocurrent dependent on light intensity are well fitted with the theoretical equations described above.

Two Schottky junctions in series may complicate the device electrical characteristics. To simplify our device and modeling, we further made devices with a single Schottky junction. Cr/Au bottom electrodes were first deposited on a SiO_2/Si substrate. A multilayer MoS_2 flake was then transferred onto the Cr/Au electrode. As the final step, Bi/Au top electrodes were deposited on top of MoS_2 (see the inset of **Figure 7a**). Au in contact with MoS_2 forms a Schottky junction and Bi in contact with MoS_2 creates an Ohmic contact. Figure 7a shows the *I–V* curves of the MoS_2 devices in Bi-Bi contact and Bi-Au contact. The MoS_2 in Bi-Bi contact has a linear *I–V* curve, indicating that the MoS_2 forms an Ohmic contact with Bi electrodes, consistent with the reports in the literature.[29,40] The MoS_2 in Bi-Au contact is nonlinear but the

 © 2024 Wiley-VCH GmbH

16136829, 2025, 6, Downloaded from https://onlinelibrary.wiley.com/doi/10.1002/smll.202408508 by Yaping Dan - Shanghai Jiaotong University , Wiley Online Library on [14/02/2025]. See the Terms and Conditions (https://onlinelibrary.wiley.com/terms-and-conditions) on Wiley Online Library for rules of use; OA articles are governed by the applicable Creative Commons License

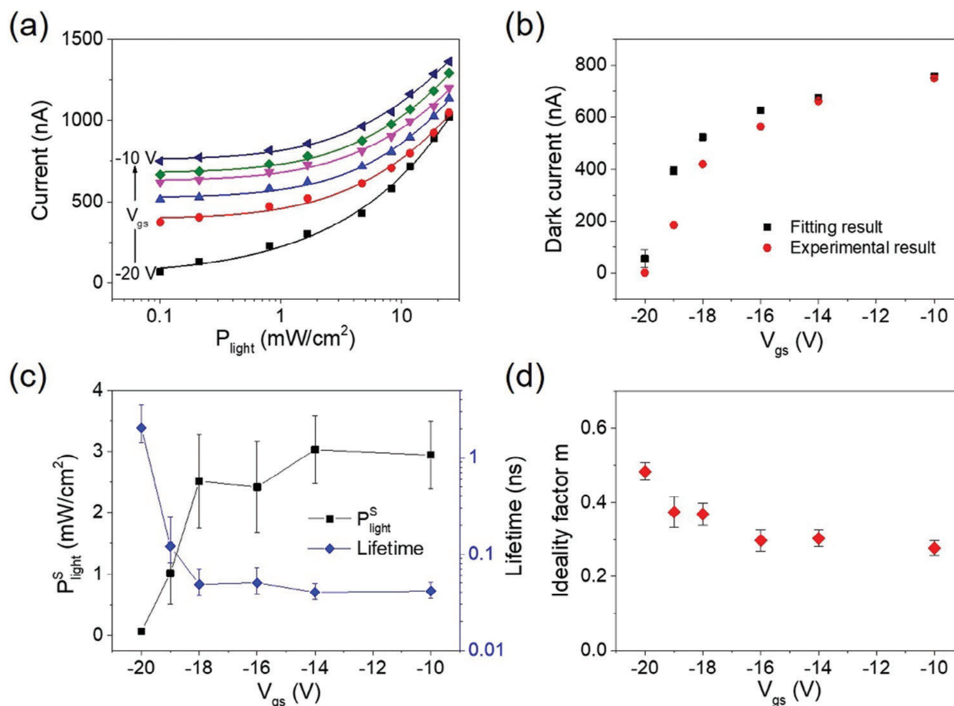

Figure 6. a) Total current under light illumination dependent on light intensity for different gate voltages. b) Extracted dark current (black squares) in comparison with experimental ones (red dots) at different gate voltage. c) Extracted critical light intensity and minority recombination lifetime at different gate voltage. d) Extracted ideality factor *m* at different gate voltages.

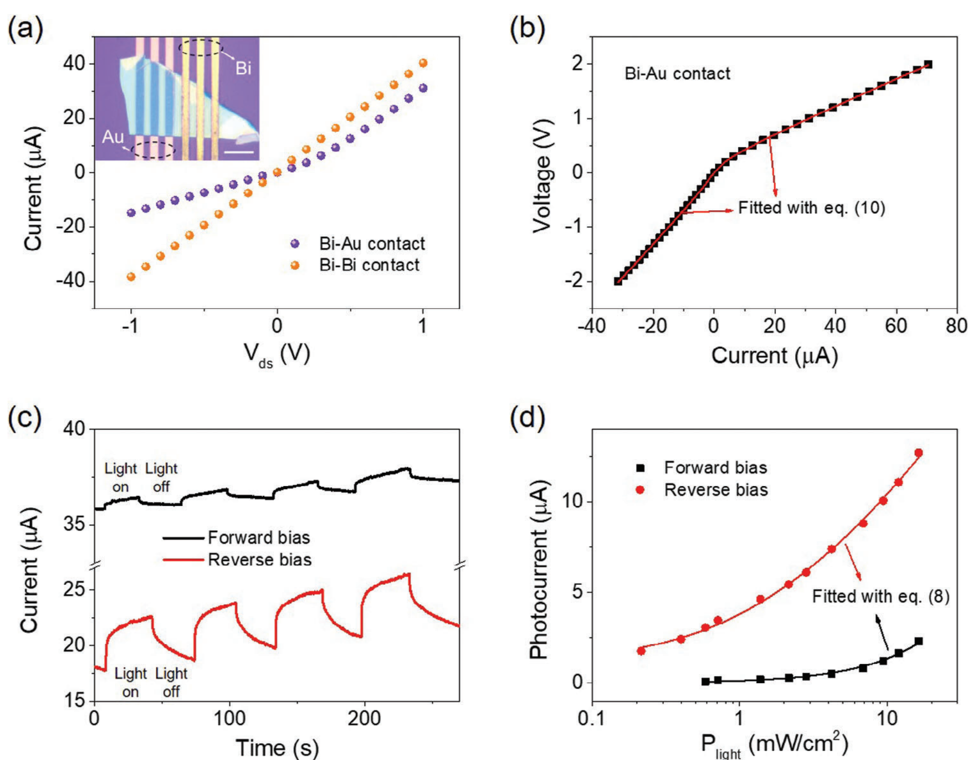

Figure 7. a) *I–V* characteristics of the device with single Schottky junction and ohmic contact. The inset is the optical image of this device, scale bar is 20 μm. b) *V–I* characteristics of the device with a single Schottky junction fitted with Equation (10). c) Current of the forward-bias (black line, $V_F = 1$ V) and reverse-bias (red line, $V_R = -1$ V) device under ON/OFF light illumination. d) Photocurrent dependent on illumination light intensity and fitting with Equation (8).

© 2024 Wiley-VCH GmbH

16136829, 2025, 6, Downloaded from https://onlinelibrary.wiley.com/doi/10.1002/smll.202408508 by Yaping Dan - Shanghai Jiaotong University , Wiley Online Library on [14/02/2025]. See the Terms and Conditions (https://onlinelibrary.wiley.com/terms-and-conditions) on Wiley Online Library for rules of use; OA articles are governed by the applicable Creative Commons License

nonlinearity is not as strong as the device in Figure 1, likely because the newly made Au-MoS_2 Schottky barrier is lower as the Schottky barrier depends on the MoS_2 thickness and the strain near the Au-MoS_2 contact.[25,26] For devices with a single Schottky junction, the I–V characteristics can be simplified as Equation (10a) for forward bias and Equation (10b) for reverse bias.

$$V_F = n\frac{kT}{q}ln\left(\frac{I}{I_s}\right) + RI \tag{10a}$$

$$V_R = \frac{n}{n-1}\,\frac{kT}{q}ln\left(\frac{I}{I_s}\right) + RI \tag{10b}$$

The experimental I–V characteristics of the single-Schottky-contact device are nicely fitted with Equation (10), shown in Figure 7b. The ideality factor n, leakage current I_s and channel resistance R of this device are extracted as 1.53, 830 nA, and 41.7 $k\Omega$, respectively, which are reasonable considering the device size and reduced Schottky barrier height. Moreover, the photoresponse of this device was also measured both in forward bias and reverse bias (Figure 7c). When the device is forward biased, the device is dominated by the channel resistance. In this case, the photoresponse is relatively weak due to the fact that the light absorption by MoS_2 is small. When the device is reverse biased, the photoresponse is stronger, because the photo-induced reduction in Schottky barrier height introduces some gain in photocurrent. We plotted the photocurrents in forward and reverse bias as a function of light intensity in Figure 7d. The experimental photoresponses can be well fitted with Equation (8). The fitting results are coherent, similar to what we observed in Figures 5 and 6.

3. Conclusion

In this work, we first established an I–V governing equation for Schottky-contact MoS_2 field effect transistors, modeled with simple components including Schottky diodes and resistors. This equation has been proved to be valid under varying conditions of gate voltage, temperature, light illumination, and bias voltage. Besides, it reveals working mechanism of 2D phototransistor to be Schottky-diodes-dominant (e.g., bias voltage <1.8 V for MoS_2 phototransistor) or channel-related-resistor-dominant (e.g., bias voltage >1.8 V for MoS_2 phototransistor). Based on that, we also established explicit analytical equations for photocurrent and photogain. It shows that ultrahigh gain are created by light-induced modulation of potential barrier ($\Delta\Phi$). Using the theory above, minority recombination lifetimes were extracted, which are consistent with the transient photoluminescence measurements. These established principles and equations are not unique to MoS_2 device and may be universally applicable to other transistors based on 2D semiconductors. In short, this work represents an important advance for device modeling and design in integrated circuits based on 2D semiconductors.

4. Experimental Section

Device Fabrication: MoS_2 devices were fabricated on a highly doped p-type Si wafer with 300 nm SiO_2. As the first step, the wafer was cleaned with acetone and deionized (DI) water. Next, the source and drain electrodes were formed on the substrate by photolithography and thermal evaporation. For the photolithography process, a negative photoresist (purchased from Futurrex Inc. in USA) was first spin-coated (4000 rpm for 40 s) on the substrate. Then the sample was transferred to a hotplate and baked at 140 °C for 1 min. Next, the sample was exposed to ultraviolet light for 14 s. After baked at 110 °C for 1 min, the sample was immersed into the developer for 15 s. Then the sample was transferred in an evaporator (Thermal Evaporator, Angstrom Engineering) and 5/50 nm thick Cr/Au was evaporated on the sample in high vacuum. A liftoff process was conducted in the acetone to create an array of Cr/Au electrodes. In the following step, a multilayer MoS_2 flake was mechanically exfoliated from a bulk MoS_2 piece and then transferred onto the target surface. Finally, the device was annealed in vacuum at 300 °C for 30 min.

Optoelectronic Measurements: A vacuum probe station was employed to provide vacuum condition for devices. High-precision digital source-meter (Keithley 2636) was used to measure the electrical properties of the devices. A 525 nm commercial LED was used as the light source, which was driven by another high-precision digital source-meter (Keithley 2400). A G10899-003 K type silicon photodiode was used to calibrate the light intensity of the LED.

Supporting Information

Supporting Information is available from the Wiley Online Library or from the author.

Acknowledgements

This work was financially supported by the Oceanic Interdisciplinary Program of Shanghai Jiao Tong University (No. SL2022ZD107), the National Natural Science Foundation of China (W2412118), the Shanghai Jiao Tong University Scientific and Technological Innovation Funds (No. 2020QY05), Science and Technology Commission of Shanghai Municipality (STCSM) Rising-Star Program (Grant 23QA1405300), Lingang Laboratory Open Research Fund (Grant LG-QS-202202-11), and the Shanghai Pujiang Program (No. 22PJ1408200). The devices were fabricated at the Center for Advanced Electronic Materials and Devices (AEMD), Shanghai Jiao Tong University.

Conflict of Interest

The authors declare no conflict of interest.

Data Availability Statement

The data that support the findings of this study are available from the corresponding author upon reasonable request.

Keywords

2D atomically thin MoS2, analytical photoresponse, photoconductors, photovoltage, schottky Junction

Received: September 19, 2024
Revised: December 16, 2024
Published online: December 29, 2024

[1] W. Zhang, J. K. Huang, C. H. Chen, Y. H. Chang, Y. J. Cheng, L. J. Li, *Adv. Mater.* **2013**, *25*, 3456.

© 2024 Wiley-VCH GmbH

16136829, 2025, 6, Downloaded from https://onlinelibrary.wiley.com/doi/10.1002/smll.202408508 by Yaping Dan - Shanghai Jiaotong University , Wiley Online Library on [14/02/2025]. See the Terms and Conditions (https://onlinelibrary.wiley.com/terms-and-conditions) on Wiley Online Library for rules of use; OA articles are governed by the applicable Creative Commons License

[2] I. Goykhman, U. Sassi, B. Desiatov, N. Mazurski, S. Milana, D. de Fazio, A. Eiden, J. Khurgin, J. Shappir, U. Levy, A. C. Ferrari, *Nano Lett.* **2016**, *16*, 3005.
[3] C. Shen, Y. Liu, J. Wu, C. Xu, D. Cui, Z. Li, Q. Liu, Y. Li, Y. Wang, X. Cao, H. Kumazoe, F. Shimojo, A. Krishnamoorthy, R. K. Kalia, A. Nakano, P. D. Vashishta, M. R. Amer, A. N. Abbas, H. Wang, W. Wu, C. Zhou, *ACS Nano* **2019**, *14*, 303.
[4] W. Yu, S. Li, Y. Zhang, W. Ma, T. Sun, J. Yuan, K. Fu, Q. Bao, *Small* **2017**, *13*, 1700268.
[5] G. H. Shin, C. Park, K. J. Lee, H. J. Jin, S. Y. Choi, *Nano Lett.* **2020**, *20*, 5741.
[6] M. Long, P. Wang, H. Fang, W. Hu, *Adv. Funct. Mater.* **2018**, *29*, 1803807.
[7] Y. Pei, R. Chen, H. Xu, D. He, C. Jiang, W. Li, X. Xiao, *Nano Res.* **2020**, *14*, 1819.
[8] J. Jiang, Y. Wen, H. Wang, L. Yin, R. Cheng, C. Liu, L. Feng, J. He, *Adv. Electron. Mater.* **2021**, *7*, 2001125.
[9] Q. Qiu, Z. Huang, *Adv. Mater.* **2021**, *33*, 2008126.
[10] K. Chen, C. Zhang, X. Zang, F. Ma, Y. Chen, Y. Dan, *Small* **2020**, *17*, 2006307.
[11] D. A. Neamen, *Semiconductor Physics and Devices: Basic Principles*, 4th ed., Mc-Graw-Hill Education, New York **2011**.
[12] Y. Dan, X. Zhao, K. Chen, A. Mesli, *ACS Photonics* **2018**, *5*, 4111.
[13] K. Chen, X. Zhao, A. Mesli, Y. He, Y. Dan, *ACS Nano* **2018**, *12*, 3436.
[14] J. He, K. Chen, C. Huang, X. Wang, Y. He, Y. Dan, *ACS Nano* **2020**, *14*, 3405.
[15] Y. Dan, Y. Lu, N. J. Kybert, Z. Luo, J. Charlie, *Nano Lett.* **2009**, *9*, 1472.
[16] K. Li, Y. Shen, Z. Su, Y. Dan, *J. Appl. Phys.* **2024**, *135*, 014301.
[17] B. Radisavljevic, A. Radenovic, J. Brivio, V. Giacometti, A. Kis, *Nat. Nanotechnol.* **2024**, *6*, 147.
[18] Y. u.-C. Lu, J.-K. Huang, K.-Y. Chao, L.-J. Li, V. P. i.-H. o. Hu, *Nat. Nanotechnol.* **2024**, *19*, 1066.
[19] X. Wang, P. Wang, J. Wang, W. Hu, X. Zhou, N. Guo, H. Huang, S. Sun, H. Shen, T. Lin, M. Tang, L. Liao, A. Jiang, J. Sun, X. Meng, X. Chen, W. Lu, J. Chu, *Adv. Mater.* **2015**, *27*, 6575.
[20] X. Guo, W. Wang, H. Nan, Y. Yu, J. Jiang, W. Zhao, J. Li, Z. Zafar, N. Xiang, Z. Ni, W. Hu, Y. You, Z. Ni, *Optica* **2016**, *3*, 1066.
[21] S.-M. Huang, S.-J. Huang, Y.-J. Yan, S.-H. Yu, M. Chou, H.-W. Yang, Y.-S. Chang, R.-S. Chen, *Sci. Rep.* **2017**, *7*, 45413.
[22] L. Ye, P. Wang, W. Luo, F. Gong, L. Liao, T. Liu, L. Tong, J. Zang, J. Xu, W. Hu, *Nano Energy* **2017**, *37*, 53.
[23] L. Viti, A. Politano, K. Zhang, M. S. Vitiello, *Nanoscale* **2019**, *11*, 1995.
[24] Y. Sun, L. Jiang, Z. Wang, Z. Hou, L. Dai, Y. Wang, J. Zhao, Y.-H. Xie, L. Zhao, Z. Jiang, W. Ren, G. Niu, *ACS Nano* **2022**, *16*, 20272.
[25] P. Sangyeon, L. Juwon, J. A-Rang, K. Seungje, P. Kyung-Ho, I. Jung, C. SeungNam, *Adv. Funct. Mater.* **2020**, *30*, 2002023.
[26] K. Soyeong, H. Min, S. Jungeun, K. Eunah, K. Youngji, R. Bo, K. H. Jerome, L. SangWook, K. Dong-Wook, *Sci. Rep.* **2019**, *9*, 14434.
[27] A. Di Bartolomeo, A. Grillo, F. Urban, L. Iemmo, F. Giubileo, G. Luongo, G. Amato, L. Croin, L. Sun, S. J. Liang, L. K. Ang, *Adv. Funct. Mater.* **2018**, *28*, 1800657.
[28] Y. Wang, J. C. Kim, R. J. Wu, J. Martinez, X. Song, J. Yang, F. Zhao, A. Mkhoyan, H. Y. Jeong, M. Chhowalla, *Nature* **2019**, *568*, 70.
[29] P.-C. Shen, C. Su, Y. Lin, A.-S. Chou, C.-C. Cheng, J.-H. Park, M.-H. Chiu, A.-Y. Lu, H.-L. Tang, M. M. Tavakoli, G. Pitner, X. Ji, Z. Cai, N. Mao, J. Wang, V. Tung, J. Li, J. Bokor, A. Zettl, C.-I. Wu, T. Palacios, L.-J. Li, J. Kong, *Nature* **2021**, *593*, 211.
[30] G. Kwon, Y.-H. Choi, H. Lee, H.-S. Kim, J. Jeong, K. Jeong, M. Baik, H. Kwon, J. Ahn, E. Lee, M. H. Cho, *Nat. Electron.* **2022**, *5*, 241.
[31] Z. Wu, Y. Zhu, F. Wang, C. Ding, Y. Wang, X. Zhan, J. He, Z. Wang, *Nano Lett.* **2022**, *22*, 7094.
[32] W. Li, X. Gong, Z. Yu, L. Ma, W. Sun, S. Gao, Ç. Köroğlu, W. Wang, L. Liu, T. Li, H. Ning, D. Fan, Y. Xu, X. Tu, T. Xu, L. Sun, W. Wang, J. Lu, Z. Ni, J. Li, X. Duan, P. Wang, Y. Nie, H. Qiu, Y. Shi, E. Pop, J. Wang, X. Wang, *Nature* **2023**, *613*, 274.
[33] A. Raja, L. Waldecker, J. Zipfel, Y. Cho, S. Brem, J. D. Ziegler, M. Kulig, T. Taniguchi, K. Watanabe, E. Malic, T. F. Heinz, T. C. Berkelbach, A. Chernikov, *Nat. Nanotechnol.* **2019**, *14*, 832.
[34] A. Grillo, A. Di Bartolomeo, *Adv. Electron. Mater.* **2021**, *7*, 2001125.
[35] C. R. Crowell, S. M. Sze, *Sohd-State Electron* **1965**, *8*, 979.
[36] H. Liu, Y. Dan, *IEEE Trans. Electron Devices* **2023**, *70*, 3630.
[37] H. Liu, K. Li, W. Zhang, Y. Dan, Explicit gain theory for pseudo polycrystalline nanowire photoconductors, in preparation.
[38] A. Castellanos-Gomez, J. Quereda, H. P van der Meulen, N. Agraït, G. Rubio-Bollinger, *Nanotechnology* **2016**, *27*, 115705.
[39] H. Liu, U. Kentsch, F. Yue, A. Mesli, Y. Dan, *J. Mater. Chem. C* **2023**, *11*, 2169.
[40] L. Kong, H. Liu, X. Wang, A. Abbas, L. Tang, M. Han, W. Li, Z. Lu, D. Lu, X. Ma, Y. Liu, Q. Liang, *Nano Lett.* **2024**, *24*, 10949.

© 2024 Wiley-VCH GmbH

16136829, 2025, 6, Downloaded from https://onlinelibrary.wiley.com/doi/10.1002/smll.202408508 by Yaping Dan - Shanghai Jiaotong University , Wiley Online Library on [14/02/2025]. See the Terms and Conditions (https://onlinelibrary.wiley.com/terms-and-conditions) on Wiley Online Library for rules of use; OA articles are governed by the applicable Creative Commons License